Available online at www.sciencedirect.com
SCIENCE DIRECT®
Journal of Power Sources 142 (2005) 92–102
JOURNAL OF POWER SOURCES
www.elsevier.com/locate/jpowsour

Simulation of a thermally coupled metal-hydride hydrogen storage and fuel cell system

Z. Jiang[a], R.A. Dougal[a], S. Liu[a], S.A. Gadre[b], A.D. Ebner[b], J.A. Ritter[b,*]

[a] *Department of Electrical Engineering, University of South Carolina, Swearingen Engineering Center, Columbia, SC 29208, USA*
[b] *Department of Chemical Engineering, University of South Carolina, Swearingen Engineering Center, Columbia, SC 29208, USA*

Received 16 August 2004; accepted 10 September 2004
Available online 8 December 2004

Abstract

For the first time, the dynamic behavior of a thermally coupled hydrogen storage and fuel cell system was studied using experimentally validated models of a metal-hydride hydrogen storage system and a proton exchange membrane (PEM) fuel cell stack. Two specific situations were studied: in the first scenario, the fuel cell and metal hydride bed were thermally coupled; in the second scenario, they were thermally uncoupled. The results from these simulations clearly exposed unique and subtle behavior associated with thermally coupled systems that could not be easily gleaned from simulating each device alone, as revealed from studying the uncoupled case. The most important result exemplified the importance of providing waste (excess) energy from the PEM fuel cell to the metal hydride bed to facilitate the removal of hydrogen during a discharge process. A detailed parametric study is forthcoming.

Keywords: Dynamic simulation; Energy systems; PEM fuel cell; Hybrid electric vehicle; Metal-hydride hydrogen storage system; Virtual test bed

1. Introduction

The use of hydrogen as an alternative to carbonaceous fuels is of increasing interest. Hydrogen exhibits very attractive features for use in applications such as hybrid electric vehicles [1], because it can be used essentially pollution-free and produced from renewable energy resources, thus eliminating the net production of greenhouse gases. Recent studies have also indicated that hydrogen costs are reasonable, which make it an ideal candidate to replace fossil fuels as an energy source [2].

Hydrogen storage has been the subject of intensive research for many years. There are currently three main technologies for storing hydrogen on vehicles: as a compressed gas, as a liquefied cryogenic fluid, and as a solid in a metal hydride [3]. The automotive industry has given considerable attention to storing hydrogen in metal hydrides because it can be stored reversibly in the solid state at relatively low pressures and ambient temperatures [4–7]. The storage vessel typically contains a powdered metal (often an alloy) that absorbs hydrogen exothermically with the concomitant release of energy as the tank is filled with hydrogen under pressure. The metal hydride desorbs the hydrogen endothermically by reducing the pressure and supplying some energy. While many applications take advantage of these properties, including rechargeable batteries [8], and heating or cooling systems [9], this paper addresses the application of metal-hydride hydrogen storage for use as a fuel in energy conversion systems such as fuel cells.

Fig. 1 illustrates a typical hydrogen-fueled energy system that is used in a hybrid electric vehicle. The fuel cell stack together with the boost converter comprises the power generation unit. The battery stores energy when the power is sufficient and releases energy when peak power is needed. When accelerating the vehicle, both the fuel cell and the

* Corresponding author. Tel.: +1 803 7773590; fax: +1 803 7778265.
E-mail address: ritter@engr.sc.edu (J.A. Ritter).

0378-7753/$ – see front matter © 2004 Elsevier B.V. All rights reserved.
doi:10.1016/j.jpowsour.2004.09.029

Nomenclature

A_{cell} effective area of each cell in the fuel cell stack (cm^2)
A_{ex} effective area of the fuel cell heat exchanger (cm^2)
$b_{j(j=1,2)}$ Henry's law constant defined in Eq. (4) ($Pa^{-1/2}$)
$b_{j0(j=1,2)}$ temperature independent coefficient of the Henry's law constant ($Pa^{-1/2}$)
C_{FC} average heat capacity of the fuel cell stack, ($J\,kg^{-1}\,K^{-1}$)
C_{pH_2} heat capacity of H_2 ($J\,mol^{-1}\,K^{-1}$)
C_{ps} heat capacity of the metal hydride ($J\,kg^{-1}\,K^{-1}$)
$d_{j(j=0,1,2)}$ coefficients in Eq. (22)
D_0 coefficient in Eq. (5)
E_{stack} voltage of the fuel cell stack (V)
E_0 standard potential of H_2–O_2 reaction (V)
f defined by Eq. (16)
F Faraday constant
h simulation step time (s)
h_{ex} overall heat transfer coefficient of the fuel cell heat exchanger ($J\,m^{-2}\,K^{-1}\,s^{-1}$)
h_{bed} overall heat transfer coefficient of the metal hydride bed heat exchanger ($J\,m^{-2}\,K^{-1}\,s^{-1}$)
ΔH isosteric heat of adsorption of the hydrogen in the metal hydride ($J\,mol^{-1}$)
ΔH_1 isosteric heat of adsorption below the switch pressure ($J\,mol^{-1}$)
ΔH_2 isosteric heat of adsorption above the switch pressure ($J\,mol^{-1}$)
ΔH_s coefficient in Eq. (5) ($J\,mol^{-1}$)
ΔH_c the heat of combustion of hydrogen ($J\,mol^{-1}$)
I the current from the fuel cell (A)
k_q mass transfer coefficient (s^{-1})
k_ρ defined by Eq. (18)
k_{C_p} defined by Eq. (19)
L length of the hydride bed (m)
m_{FC} mass of the fuel cell stack (kg)
M_{MH} average molecular weight of metal hydride ($kg\,mol^{-1}$)
N number of the cells in the fuel cell stack
m hydrogen flow rate out of the metal hydride bed ($mol\,s^{-1}$)
$n_{j(j=0,1,2)}$ coefficients in Eq. (22)
$\dot{n}$ hydrogen flow rate ($mol\,s^{-1}$)
P pressure inside the metal hydride bed (Pa)
P_0 pressure inside the metal hydride bed at the initial state (Pa)
P_{FC} pressure of the hydrogen in the fuel cell (Pa)
P_s equilibrium pressure of the hydrogen in the metal hydride bed at the envelope (Pa)
q hydrogen concentration in the metal hydride ($mol\,mol^{-1}$)
q^* equilibrium hydrogen concentration in the metal hydride ($mol\,mol^{-1}$)
q_{max} maximum equilibrium hydrogen concentration in the metal hydride ($mol\,mol^{-1}$)
$q_0{}^*$ equilibrium hydrogen concentration in the metal hydride at the initial state ($mol\,mol^{-1}$)
q_s saturation hydrogen concentration in the metal hydride at the low concentration phase ($mol\,mol^{-1}$)
Q rate of energy exchange with the metal hydride bed ($J\,s^{-1}\,m^{-3}$)
$r_{j(j=0,1,2)}$ coefficients in Eq. (22)
R ideal gas constant ($J\,mol^{-1}\,K^{-1}$)
R_i radius of the metal hydride bed heat exchanger tube (m)
R_o radius of the outer wall of the metal hydride bed (m)
t time (s)
T average temperature of the hydrogen inside the metal hydride bed (K)
T_{amb} the temperature of the ambient (K)
T_0 average temperature of the hydrogen inside the metal hydride bed at the initial state (K)
T_m temperature of the heat transfer medium for the metal hydride bed (K)
T_{FC} the bulk temperature of the fuel cell stack (K)
V_b volume of the metal hydride bed (m^3)
$\dot{W}_{amb}$ thermal power transferred from the fuel cell to the ambient environment (W)
$\dot{W}_e$ electrical power released from the fuel cell (W)
$\dot{W}_{th}$ thermal power generated by the fuel cell (W)

Greek symbols
ε metal hydride bed porosity, dimensionless
ρ_s density of the metal hydride ($kg\,m^{-3}$)
v_1 rate of pressure change inside the metal hydride bed ($Pa\,s^{-1}$)
v_2 rate of average temperature change of the hydrogen in the metal hydride bed ($K\,s^{-1}$)
v_3 rate of H_2 concentration change inside the metal hydride bed ($mol\,mol^{-1}\,s^{-1}$)

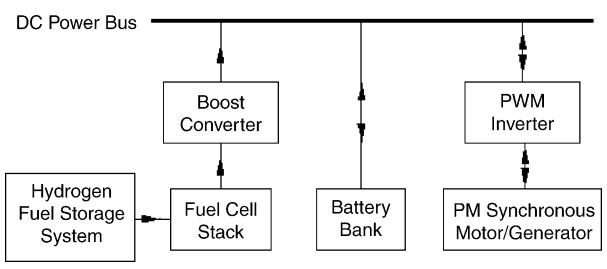

Fig. 1. Block diagram of a typical hydrogen-fueled energy system that is used in a hybrid electric vehicle.

battery provide electrical power to the permanent magnet (PM) synchronous motor through the PWM inverter. When decelerating the vehicle, the motor acts as a generator and the generated power is used to charge the battery. The hydrogen storage system provides hydrogen for the fuel cell stack as necessary.

When hydrogen is released from the metal hydride bed, the endothermic desorption process causes its temperature to decrease [10]. In turn, this decrease in temperature greatly diminishes the rate at which hydrogen can be released from the bed. To ameliorate this undesirable effect, some of the excess heat naturally produced from the fuel cell during the generation of electricity can be transferred to the metal hydride bed to increase its temperature. In other words, the metal hydride bed can be thermally coupled to the fuel cell stack, which not only facilitates the release of hydrogen from the metal hydride bed, but it also helps remove excess (waste) heat from the fuel cell stack.

The objective of this paper is to study, for the first time, the behavior of a thermally coupled hydrogen storage and fuel cell system. This system level simulation is carried out using a very friendly computational environment refereed to as the virtual test bed (VTB) [11–14], along with suitable models that describe the dynamic performances of the metal hydride bed and fuel cell stack with enough rigor to capture the physics but not overwhelm the system simulator. Although many detailed models of a metal hydride bed have been developed to study the dynamics inside the bed [10,15–17], only that developed recently by Gadre et al. [10] has been validated against extensive experimental data and is simple enough for system level studies [10]. For similar reasons, a relatively simple proton exchange membrane (PEM) fuel cell model is chosen here for these system studies [18].

First, the inherently nonlinear model equations that realistically account for heat and mass transfer resistances associated with the discharge of hydrogen from a metal hydride bed [10] are reformulated in a resistive companion (RC) form for efficient solution in the VTB platform [13]. Then the PEM fuel cell model [18] is dynamically coupled to the RC form of the metal hydride bed model in the VTB environment. System-level simulations of the resulting integrated metal-hydride hydrogen storage and fuel cell system are then carried out for both thermally coupled and uncoupled scenarios. These two scenarios expose the advantages of providing waste or excess energy from the PEM fuel cell stack to the metal hydride bed to facilitate the removal of hydrogen.

2. Metal-hydride hydrogen system model

The metal hydride bed under study consists of a cylindrical container of radius R_o filled with a metal powder that chemically absorbs the hydrogen under pressure. This container also has an internal co-axial heat exchanger of radius R_i that supplies the energy needed to release the hydrogen during discharge and carries away excess heat during charge. Appropriate assumptions are made so that the distributed thermal and mass transfer phenomena that occur within this vessel are described by lumped approximations that still allow for a realistic but less complicated description of this complex process. First, it is assumed that the system is symmetric around the bed axis and that all the variables vary along the bed according to plug flow conditions, i.e., with no radial gradients. Similarly, axial gradients of temperature and pressure are neglected while the gas molar flux in the bed is assumed to vary linearly from a value of zero at the closed end of the bed. Identical temperatures are assumed for both the solid and gas phases. The external surface is assumed to be perfectly insulated, and heat transfer between the bed and the internal heat exchanger is described by an overall heat transfer coefficient. The temperature inside the heat exchanger is assumed to be constant along the bed and throughout the hydrogen desorption process. The mass transfer resistance in the solid phase is described by a linear driving force (LDF) approximation, using a mass transfer coefficient that is assumed to be independent of temperature. The desorption process starts from a fully charged, equilibrium state at a given initial temperature and pressure. Throughout the process, it is assumed that the flow rate at the discharge end of the bed, i.e., the molar flux, is defined either as a constant or as a time dependent function.

Based on these assumptions and assuming ideal gas behavior, the one-dimension mass balance is governed by

$$\frac{1}{RT}\frac{\partial P}{\partial t} - \frac{P}{RT^2}\frac{\partial T}{\partial t} + \frac{\dot{n}}{\pi(R_o^2 - R_i^2)L} + \frac{1-\varepsilon}{\varepsilon}\frac{\rho_s}{2M_{MH}}\frac{\partial q}{\partial t} = 0 \tag{1}$$

where P is the pressure inside the bed, T the average temperature of the hydrogen in the metal hydride bed, R the universal gas constant, $\dot{n}$ the hydrogen flow rate demand, R_i the radius of the heat exchanger tube, R_o the radius of the bed, L the length of the bed, ε the porosity of the metal hydride bed, ρ_s the density of the metal hydride, M_{MH} the average molecular weight of the metal hydride, and q is the hydrogen concentration in the metal hydride. The corresponding energy balance, including expansion/compression effects, but ignoring convection effects (as it contains no spatial gradients), is written as

$$\left(\frac{P}{RT}C_{pH_2} + \frac{1-\varepsilon}{\varepsilon}\rho_s C_{ps}\right)\frac{\partial T}{\partial t} + \frac{\partial P}{\partial t} + \frac{1-\varepsilon}{\varepsilon}\frac{\rho_s \Delta H}{2M_{MH}}\frac{\partial q}{\partial t} + \frac{2h_{bed}R_i}{\varepsilon(R_o^2 - R_i^2)}(T - T_m) = 0 \tag{2}$$

where C_{pH_2} is the heat capacity of the hydrogen, C_{ps} the heat capacity of the metal hydride, ΔH the isosteric heat of adsorption of the hydrogen in the metal hydride, h_{bed} the overall heat transfer coefficient of the metal hydride bed heat exchange, and T_m is the temperature of the metal hydride bed heat exchanger exchange medium. The intraparticle mass transfer

mechanism is based on the following LDF expression:

$$\frac{\partial q}{\partial t} = k_q(q^* - q) \tag{3}$$

where q^* is the concentration of hydrogen in the metal hydride in equilibrium with the gas phase at P and T, and k_q is the mass transfer coefficient.

The thermodynamic relationship that describes the equilibrium loading of hydrogen in the metal hydride as a function of pressure and temperature, the so called pressure–composition–temperature (PCT) relationship, can be adequately represented by the composite Langmuir model [10]. This thermodynamic model consists of two Langmuir-type isotherms connected at a so-called switch point, i.e.,

$$q^* = \begin{cases} \dfrac{q_s\left(1 + b_1\sqrt{P_s}\right)}{\left(1 + b_1\sqrt{P}\right)}\dfrac{\sqrt{P}}{\sqrt{P_s}}, & P \le P_s(T) \\ q_s + \dfrac{(q_{max} - q_s)b_2\left(\sqrt{P} - \sqrt{P_s}\right)}{\left(1 + b_2(\sqrt{P} - \sqrt{P_s})\right)}, & P > P_s(T) \end{cases} \tag{4}$$

where $b_1 = b_{1o}\exp\left(-\frac{\Delta H_1}{RT}\right)$, $b_2 = b_{2o}\exp\left(-\frac{\Delta H_2}{RT}\right)$, ΔH_1 and ΔH_2 are the heats of adsorption below and above the switch point, and q_{max}, b_{1o}, and b_{2o} are fitting parameters. P_s and q_s are the switch pressure and hydrogen concentration in the metal hydride that correspond to the point on the isotherm where the phase transition starts. The switch variable P_s is related to T according to

$$\ln(P_s) = D_o + \frac{\Delta H_s}{RT} \tag{5}$$

where D_o and ΔH_s are additional fitting parameters. Due to the composite nature of the Langmuir isotherm model, the isosteric heat of adsorption of the hydrogen in the metal hydride is evaluated distinctively depending on whether the pressure is below or above P_s, i.e.,

$$\Delta H = \begin{cases} 2\Delta H_1 = \Delta H_s & , P \le P_s(T) \\ 2\left[\Delta H_2 + (\Delta H_1 - \Delta H_2)\frac{\sqrt{P_s}}{\sqrt{P}}\right] & , P > P_s(T) \end{cases} \tag{6}$$

To complete the description of the model, the following initial conditions are needed: at $t = 0$, $P = P_0$, $T = T_0$, and $q = q_0 = q_0{}^*$.

Eqs. (1)–(6) constitute a relatively simple mathematical model that realistically accounts for heat and mass transfer resistances during the dynamic discharge of hydrogen from a metal hydride bed. It should be noted that this model is a simplified version of a complete set of validated equations that describe the dynamics of the hydrogen discharge process over a wide range of hydrogen flow rates [10]. The main difference is that axial temperature gradients (i.e., convection effects) are ignored in this simplified version.

This resistive companion (RC) method was applied to the system of equations to yield a form of the model that is amenable to "natural coupling," i.e., a form of the model that can be inserted into a network without regard to causality [13,14]. Natural conservation laws are automatically enforced where appropriate. As shown above, Eqs. (1)–(3) are nonlinear differential equations. The construction of the RC model for the metal hydride bed begins by introducing three intermediate variables to replace the derivative terms in the system equations by defining

$$v_1 = \frac{\partial P}{\partial t} \tag{7}$$

$$v_2 = \frac{\partial T}{\partial t} \tag{8}$$

$$v_3 = \frac{\partial q}{\partial t} \tag{9}$$

where v_1, v_2, and v_3 are intermediate variables. Integrating Eq. (7) over one time step, i.e., from time instant $(t - h)$ to t, allows it to be expressed in discrete form as,

$$[v_1(t) + v_1(t - h)]\frac{h}{2} = P(t) - P(t - h) \tag{10}$$

where t is the current simulation time, and h is the simulation time step. Rearranging Eq. (10) yields

$$0 = P(t) - \frac{h}{2}v_1(t) - \left[P(t - h) + \frac{h}{2}v_1(t - h)\right] \tag{11}$$

Similarly, discretizing Eqs. (8) and (9) and rearranging gives the following equations:

$$0 = T(t) - \frac{h}{2}v_2(t) - \left[T(t - h) + \frac{h}{2}v_2(t - h)\right] \tag{12}$$

$$0 = q(t) - \frac{h}{2}v_3(t) - \left[q(t - h) + \frac{h}{2}v_3(t - h)\right] \tag{13}$$

Eqs. (11)–(13) are in the standard RC form. Based on the definitions given in Eqs. (7)–(9), Eqs. (1)–(3) are then converted to three nonlinear algebraic equations as follows.

$$m = \frac{k_m v_1}{RT} - \frac{k_m P}{RT^2}v_2 + k_m k_\rho v_3 \tag{14}$$

$$Q = k_m\varepsilon\left(\frac{P}{RT}C_{pH_2} + k_{C_p}\right)v_2 + k_m\varepsilon\, v_1 + k_m\varepsilon\, k_\rho\, \Delta H\, v_3 \tag{15}$$

$$f = v_3 - k_q(q^* - q) = 0 \tag{16}$$

where Q is the rate of heat exchange between the metal hydride bed and its heat exchanger, m the molar flow out of the hydride bed, V_b the volume of the metal hydride bed, and k_ρ and k_{C_p} are given by Eqs. (17)–(21).

$$Q = 2h_{bed}\pi\, R_i\, L(T_m - T) \tag{17}$$

$$k_\rho = \frac{1 - \varepsilon}{\varepsilon}\frac{\rho_s}{2M_{MH}} \tag{18}$$

$$k_{C_p} = \frac{1 - \varepsilon}{\varepsilon}\rho_s C_{p_s} \tag{19}$$

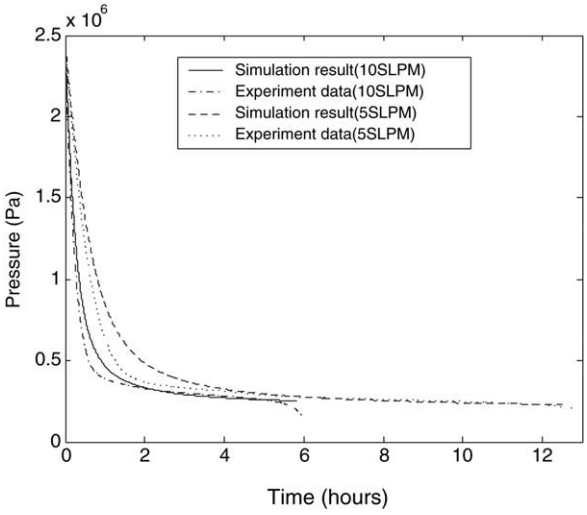

Fig. 2. Model predictions of the experimental pressure histories [10] in the metal hydride bed for hydrogen flow rate demands of 5 and 10 SLPM.

$$k_{\mathrm{m}} = \pi(R_{\mathrm{o}}^2 - R_{\mathrm{i}}^2)L \tag{20}$$

$$m = -\dot{n} \tag{21}$$

The RC equations are written in matrix form, including the conductance matrix and history vector. In this RC form, the dynamic model of the metal hydride bed is easily implemented in the VTB, with seamless integration between other components and devices of interest, like the fuel cell stack.

Figs. 2 and 3, respectively, compare the experimental pressure and temperature histories [10] with those obtained from the RC form of the metal hydride bed model for hydrogen flow rate demands of 5 and 10 SLPM (standard liter per minute). The results in Fig. 2 show that the dynamic pressure behavior is predicted quite well by the RC form of the model, especially during the periods where the pressure remains relatively constant. The minor discrepancies observed just before the pressure begins to level off are most likely associated with the one-dimensional model not accounting for the convection of energy in the axial direction, as noted earlier. This becomes more apparent in the prediction of the temperature histories shown in Fig. 3. The RC form of the model does quite well in predicting the temperature history for the 5 SLPM hydrogen flow rate demand, but begins to deviate a bit more at the higher hydrogen flow rate demand of 10 SLPM, but still less than 1 K. It can therefore be stated that, for hydrogen flow rate demands on the order of 10 SLPM or less, where the heat effects are not so drastic, the RC form of the model is quite sufficient for use to study the performance of dynamically coupled systems.

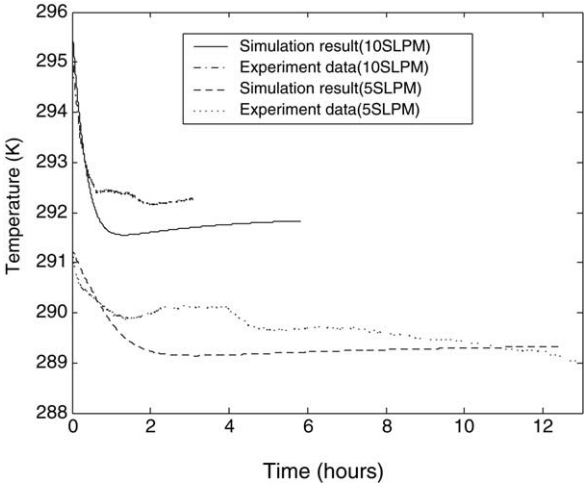

Fig. 3. Model predictions of experimental temperature histories [10] in the metal hydride bed for hydrogen flow rate demands of 5 and 10 SLPM.

3. Proton exchange membrane (PEM) fuel cell model

The main power source of the integrated, hydrogen-fueled fuel cell system is a 25-cell PEM fuel cell stack with the cells organized in series. The voltage of each cell varies with the current, temperature and pressure according to the empirical equation shown below [18].

$$E_{\mathrm{stack}} = N\left[E_0 - (b_0 T_{\mathrm{FC}}^2 + b_1 T_{\mathrm{FC}} + b_2)\log\left(\frac{I}{A_{\mathrm{cell}}}\right) - (r_0 T_{\mathrm{FC}}^2 + r_1 T_{\mathrm{FC}} + r_2))\frac{I}{A_{\mathrm{cell}}} - (m_0 P_{\mathrm{FC}}^2 + m_1 P_{\mathrm{FC}} + m_2)\exp\left((n_0 P_{\mathrm{FC}}^2 + n_1 P_{\mathrm{FC}} + n_2)\frac{I}{A_{\mathrm{cell}}}\right)\right] \tag{22}$$

where E_0 is the standard potential of H_2–O_2 reaction, I the current from the fuel cell, E_{stack} the voltage of the fuel cell stack, N the number of cells, A_{cell} the area of each cell, T_{FC} the bulk temperature of the fuel cell stack, and P_{FC} is the hydrogen pressure in the fuel cell. Constants b_i, r_i, m_i, and n_i ($i = 0, 1, 2$) are coefficients determined empirically from experimental data. This fuel cell model was also validated against experimental data elsewhere [18] (also refer to the online document [11]).

The relationship between the hydrogen molar flow rate $\dot{n}$ and the current I generated by the fuel cell is given by

$$I = \frac{2\dot{n}F}{N} \tag{23}$$

where F is the Faraday constant. The thermal power $\dot{W}_{\mathrm{th}}$ generated by the fuel cell is given by the following formula:

$$\dot{W}_{\mathrm{th}} = \dot{n}\Delta H_{\mathrm{c}} - \dot{W}_{\mathrm{e}} \tag{24}$$

where ΔH_{c} is the heat of combustion of hydrogen and $\dot{W}_{\mathrm{e}}$ the electrical power generated by the fuel cell. Also, the thermal power released from the fuel cell stack is divided into two parts: some is transferred to the metal hydride bed, and the rest is transferred to the ambient environment. This situation is denoted by:

$$\dot{W}_{\mathrm{th}} = Q + \dot{W}_{\mathrm{amb}} + C_{\mathrm{FC}} m_{\mathrm{FC}} \frac{\mathrm{d}T_{\mathrm{FC}}}{\mathrm{d}t} \tag{25}$$

where C_{FC} is the average heat capacity of the fuel cell stack, m_{FC} is the mass of the fuel cell stack, and $\dot{W}_{amb}$ is the thermal power transferred between the fuel cell heat exchanger and the ambient environment according to

$$\dot{W}_{amb} = h_{ex} A_{ex} (T_{FC} - T_{amb}) \quad (26)$$

where h_{ex} is the overall heat transfer coefficient of the fuel cell heat exchanger and A_{ex} is the effective area of the heat exchanger. The fuel cell stack voltage and current are related to the electrical power generated by the fuel cell by

$$\dot{W}_e = E_{stack} I \quad (27)$$

4. System level simulation in the VT environment

System level simulations of the hydrogen-fueled, fuel cell system were carried out with and without the fuel cell being thermally coupled to the metal hydride bed. In both situations the metal hydride bed is connected to the fuel cell through a pressure regulator to supply hydrogen at 1.0 atm constant pressure. Air is also fed to the fuel cell at 1.0 atm constant pressure. For the uncoupled simulations, both the fuel cell and the metal hydride bed are configured to independently exchange heat with the ambient environment (i.e., the temperature source). This integrated, but thermally uncoupled hydrogen storage and fuel cell energy system is shown schematically in the VTB environment in Fig. 4a. The water circulating through the metal hydride bed and the fuel cell heat exchangers (labeled 1 and 2, respectively) in this case is held constant at 296 K, the ambient temperature. For the coupled simulations, the metal hydride bed is configured to exchange energy with the fuel cell stack through a heat exchanger, since the fuel cell produces excess (waste) heat during operation. Fig. 4b shows the VTB environment schematic of this integrated and now thermally coupled hydrogen storage and fuel cell energy system. Except for the heat transfer between the metal hydride bed and the fuel cell being coupled, the rest of the system is identical to that shown in Fig. 3. However, in this case, the temperature of the recirculating water is assumed to be equal to the bulk temperature of the fuel cell. The values of all the parameters used in the model equations are given in Tables 1 and 2.

For the thermally coupled case, 11 equations, namely Eqs. (4), (14)–(17), and (22)–(27), were solved simultaneously for 11 unknowns, namely, E_{stack}, I, $\dot{n}$, P, q, q^*, Q, T, T_{FC}, $\dot{W}_{amb}$ and $\dot{W}_{th}$. Also, for this coupled case, the temperature of the metal hydride bed heat exchanger medium T_m in Eq. (17) becomes T_{FC}. For the uncoupled case, the same set of equations and unknowns are solved simultaneously; however, Eq. (25) is no longer valid because Q does not exchange energy with the fuel cell but instead with the ambient environment. In this case, Eq. (25) simply becomes $\dot{W}_{th} = \dot{W}_{amb}$ and the temperature of the metal hydride bed heat exchanger medium T_m in Eq. (17) becomes T_{amb}.

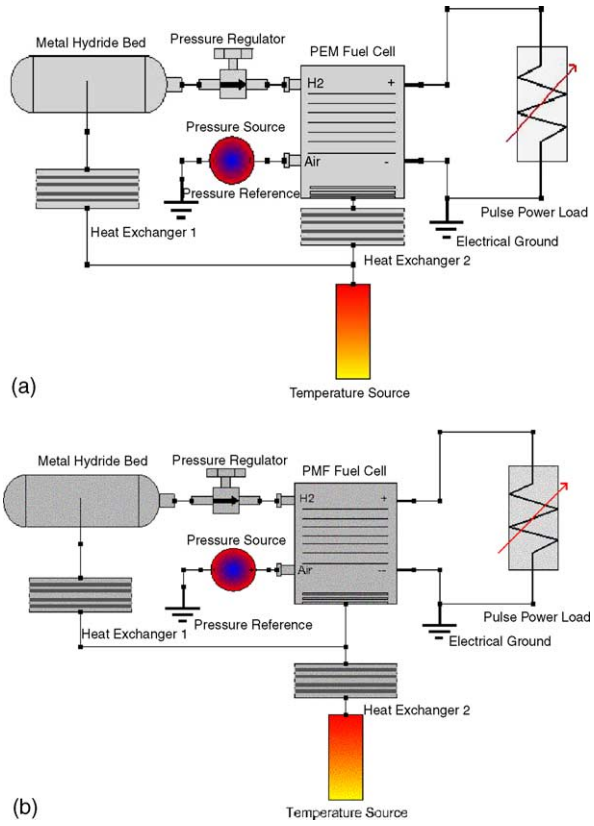

Fig. 4. Schematics of thermally uncoupled and thermally coupled hydrogen storage and fuel cell systems in the VTB environment: (a) thermally uncoupled system and (b) thermally-coupled system.

In both the uncoupled and coupled simulations, a pulse power load ($\dot{W}_e$) draws 200 W for 0.25 h and then 100 W for 0.25 h alternately from the fuel cell for 4 h, as shown in Fig. 5. The corresponding voltage and temperature of the fuel cell stack are given in Figs. 6 and 7, respectively. Fig. 8 shows the thermal power released from the fuel cell during operation of

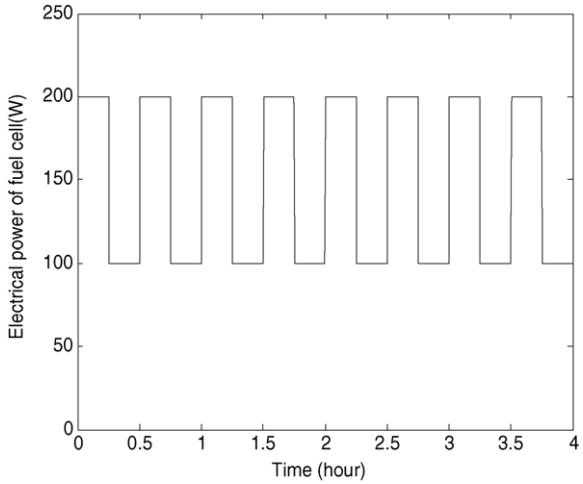

Fig. 5. Pulsed power drawn from the fuel cell stack, alternating between 200 W and 100 W every 0.5 h for 4 h of operation, whether thermally coupled to the metal hydride bed or not.

Table 1
Model parameters used in the fuel cell and metal hydride bed simulations [10]

Parameter	Value
A_{ex} (cm^2)	2.00E+2
A_{cell} (cm^2)	2.00E+2
b_{10} ($Pa^{-1/2}$)	2.36E−6
b_{20} ($Pa^{-1/2}$)	7.87E−6
C_{FC}* ($J\,K^{-1}\,kg^{-1}$)	8.13E+2
C_{pH_2} ($J\,mol^{-1}\,K^{-1}$)	2.88E+1
C_{ps} ($J\,mol^{-1}\,K^{-1}$)	4.20E+2
D_0	2.40E+1
E_0 (V)	1.00E+0
F ($C\,mol^{-1}$)	9.65E+4
h_{bed} ($W\,m^{-2}\,K^{-1}$)	7.57E+1
h_{ex} ($W\,m^{-2}\,K^{-1}$)	1.70E+2
k_q (s^{-1})	8.14E−3
L (m)	1.52E+0
m_{FC}* (kg)	1.72E+0
M_{MH} ($kg\,mol^{-1}$)	7.29E−2
P_0 (Pa)	5.05E+6
P_{FC} (Pa)	1.01E+5
q_{max} ($mol\,mol^{-1}$)	9.84E−1
q_s ($mol\,mol^{-1}$)	1.25E−1
R ($J\,mol^{-1}\,K^{-1}$)	8.31E+0
R_i (m)	2.00E−2
R_o (m)	4.50E−2
T_{amb} (K)	2.96E+2
T_c (K)	2.96E+2
T_0 (K)	2.96E+2
ε	5.28E−1
ρ_s ($kg\,m^{-3}$)	7.61E+3
N	2.50E+1
ΔH_1 ($J\,mol^{-1}$)	−1.38E+4
ΔH_2 ($J\,mol^{-1}$)	−206E+4
ΔH_s ($J\,mol^{-1}$)	−2.77E+4
ΔH_c ($J\,mol^{-1}$)	−2.42E+5

* Based on [19,20].

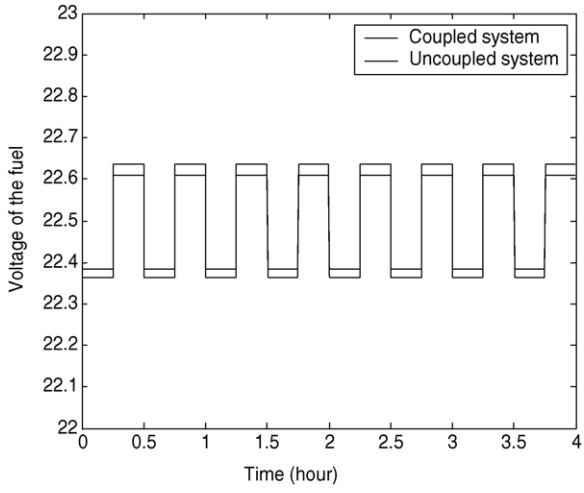

Fig. 6. Voltage of the fuel cell stack during pulsed operation of the fuel cell while thermally coupled and uncoupled to the metal hydride bed.

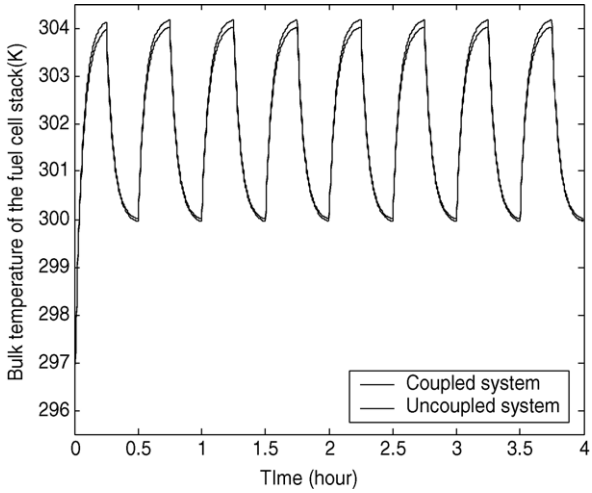

Fig. 7. Temperature of the fuel cell stack during pulsed operation of the fuel cell while thermally coupled and uncoupled to the metal hydride bed.

the fuel cell over the 4 h for both uncoupled and coupled operations. The hydrogen flow rate demand and the cumulative percentage of the hydrogen in the metal hydride bed consumed over this 4 h period are shown in Fig. 9. Figs. 10–12, respectively, display the corresponding hydrogen loading in the solid metal hydride phase, the metal hydride bed pressure, and the metal hydride bed temperature histories for both the uncoupled and coupled systems. Finally, Fig. 13 shows the thermal power transferred to the metal hydride bed from the fuel cell over the 4 h for both the uncoupled and coupled operations.

During the 4 h period of pulsed operation of the fuel cell, with a load alternately drawing 200 W and 100 W every 0.25 h, the fuel cell operates at nearly a constant voltage of 22.5 ± 0.1 V (Fig. 6). The 0.1 V periodic swing is due to the high and low power levels, with the higher voltage naturally corresponding to the lower power level. The uncoupled system also operates at a marginally higher voltage, most likely due to the effect of thermal coupling on the fuel cell temperature during pulsed operation.

Fig. 7 shows that during this 4 h period, the fuel cell temperature, initially starting from 296 K, exhibits essentially a

Table 2
Values of the polynomial coefficients used in the PEM fuel cell model [18]

Coefficient	Value
d_0 ($mV\,K^{-2}\,cell^{-1}$)	3.09E−3
d_1 ($mV\,K^{-1}\,cell^{-1}$)	−2.05E+0
d_2 ($mV\,cell^{-1}$)	4.60E+2
r_0 ($\Omega\,cm^2\,K^{-2}\,cell^{-1}$)	1.52E−5
r_1 ($\Omega\,cm^2\,K^{-1}\,cell^{-1}$)	−1.00E−2
r_2 ($\Omega\,cm^2\,cell^{-1}$)	2.50E+0
m_0 ($mV\,Pa^{-2}\,cell^{-1}$)	1.31E−11
m_1 ($mV\,Pa^{-1}\,cell^{-1}$)	−7.33E−6
m_2 ($mV\,cell^{-1}$)	1.05E+0
n_0 ($cm^2\,mA^{-1}\,Pa^{-2}$)	−2.84E−13
n_1 ($cm^2\,mA^{-1}\,Pa^{-1}$)	1.16E−7
n_2 ($cm^2\,mA^{-1}$)	−6.39E−3

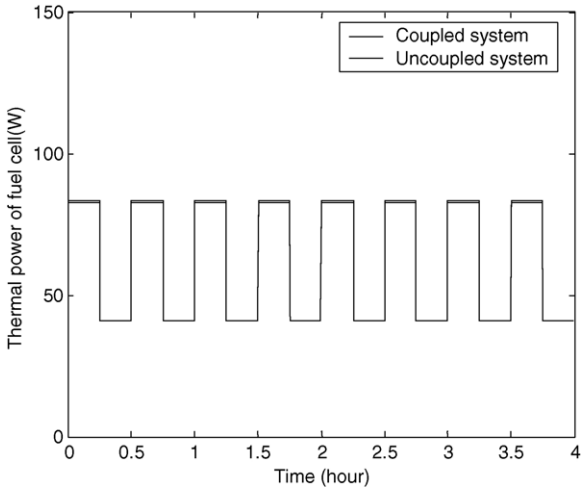

Fig. 8. Thermal power released from the fuel cell to the ambient environment during uncoupled operation, and to the ambient environment and the metal hydride bed during coupled operation.

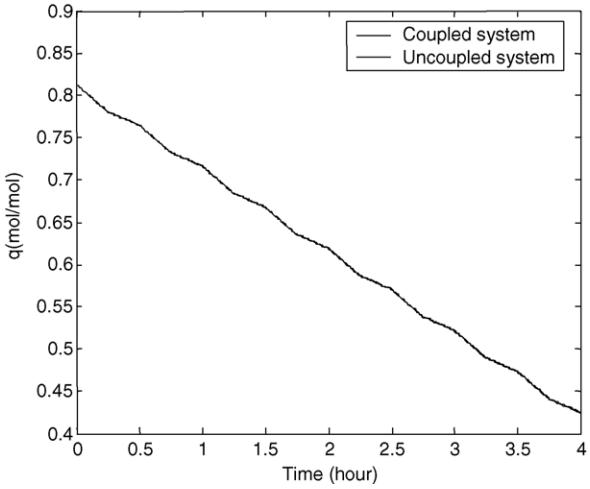

Fig. 10. Hydrogen loading in the solid metal hydride phase in the metal hydride bed during pulsed operation of and while thermally coupled and uncoupled to the fuel cell.

saw tooth pattern and oscillates between 304 K and 300 K corresponding to the high and low power periods, respectively. It is noteworthy that a slightly higher temperature is observed for the uncoupled operation especially during the high power periods. This suggests that more energy is being removed from the fuel cell when the metal hydride bed is thermally coupled to the fuel cell, a very positive but in this case a very minor effect. This result is further substantiated in Fig. 8, which shows that during coupled operation, slightly more energy is transferred from the fuel cell during high power operation. Fig. 8 also shows that during the 4 h period of pulsed operation, with the load varying between 200 W and 100 W, approximately 80 W and 40 W of power are respectively converted into waste heat. This means that 60% of the energy obtained from the hydrogen is converted into useful electricity. The other 40% of the energy is converted into waste heat, with no other energy losses accounted for in this system simulation. This brings up one of the main questions addressed in this work: what is the effect of transferring some of this waste energy from the fuel cell to the metal hydride bed.

Fig. 9 shows that during the 4 h of pulsed operation the fuel cell consumes a little more than 50% of the total hydrogen in the bed, with the hydrogen flowing at constant but alternating rates of 1.2 and 0.6 SLPM, respectively and proportionally, corresponding to the high and low power levels. However, the hydrogen consumption is the same whether the metal hydride bed is thermally coupled to the fuel cell or not, which is clearly reflected in the change in the hydrogen loading in the metal hydride phase. Fig. 10 shows that it decreases from about 0.81 mol mol^{-1} to 0.43 mol mol^{-1}. Hence, a little less than half of the hydrogen in the solid (metal hydride) phase is consumed during 4 h of operation; accounting also for the

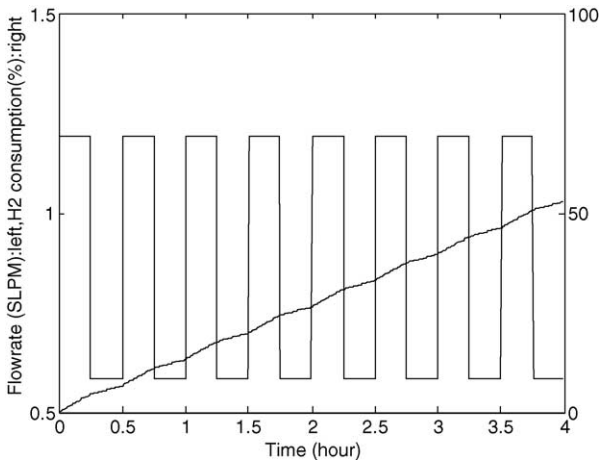

Fig. 9. Hydrogen flow rate demand and cumulative percentage of initial hydrogen in the metal hydride bed consumed over the 4 h period of pulsed operation of the fuel cell whether coupled to the metal hydride bed or not.

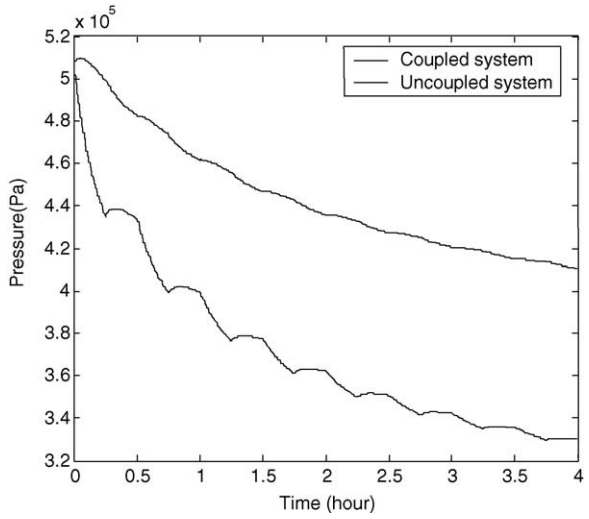

Fig. 11. Gas phase pressure inside the metal hydride bed during pulsed operation of and while thermally coupled and uncoupled to the fuel cell.

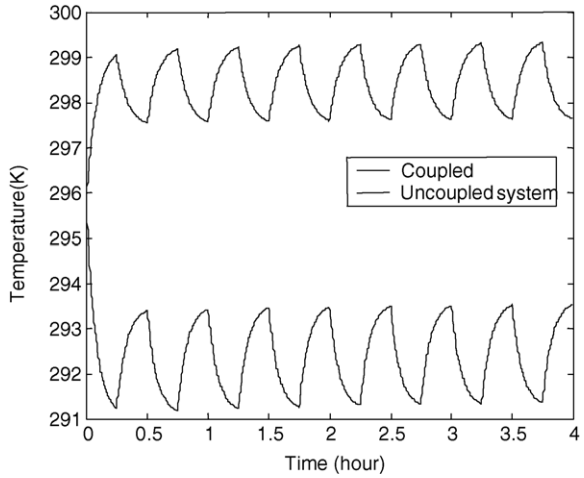

Fig. 12. Average bulk temperature of the metal hydride bed during pulsed operation of and while thermally coupled and uncoupled to the fuel cell.

hydrogen in the gas phase brings the total hydrogen consumed to a little more than 50% as stated above and shown in Fig. 9. So, as may be expected, thermally coupling the system does not affect the hydrogen flow rate, which is dictated by the power requirements of the load imparted to the fuel cell. It also does not affect the hydrogen loading in the metal hydride phase, a result that is not so obvious but is easily rationalized because this is the source of the hydrogen. What thermally coupling does effect is the temperature of the metal hydride bed, which in turn effects the pressure of the bed. These effects are clearly observed in Figs. 11 and 12. The different curves in these figures reflect the differences observed when the metal hydride bed exchanges energy with the ambient environment (uncoupled) compared to when it exchanges energy with the fuel cell (coupled), as shown in Fig. 13.

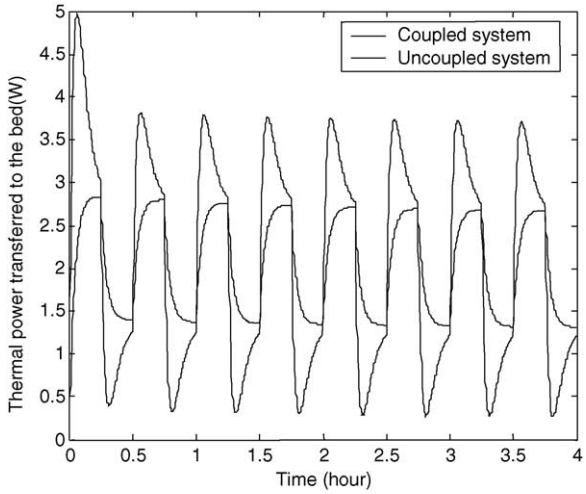

Fig. 13. Thermal power transferred to the metal hydride bed from the ambient environment during uncoupled operation and from the fuel cell during coupled operation.

For the uncoupled case, the pressure inside the bed decreases from about 5.0×10^5 Pa to about 3.3×10^5 Pa. However, in the coupled case, the pressure inside the bed decreases much less from about 5.0×10^5 Pa to only about 4.1×10^5 Pa over the same 4 h of operation. This is due to the more energy, on average, being transferred to the metal hydride bed when the bed is thermally coupled with the fuel cell (about 3 W, net) compared to when it is thermally coupled with the ambient environment (about 1 W net), as shown in Fig. 13. This small amount of extra energy causes the temperature and hence the pressure of the metal hydride bed to both increase, with the temperature cycling between 297.6 K and 299.2 K. Although these temperatures are always above the ambient temperature of 296 K, this is not the temperature of interest for the coupled case; the temperature of interest is the fuel cell temperature, which varies between 300 K and 304 K (Fig. 7). Hence, the metal hydride bed is always operating below the fuel cell temperature, which means that energy is always being transferred to the bed (Fig. 13), a positive effect. In contrast, for the uncoupled case, the metal hydride bed temperature is always below the ambient temperature, cycling between 291.3 K and 293.5 K. In this case, the ambient temperature is the temperature of interest, and again with the bed always operating below the ambient temperature, energy is being transferred to the bed (Fig. 13). However, the higher operating temperature of the thermally coupled metal hydride bed translates into a greater time during which the fuel cell may continue to produce 200 W and 100 W of useful power. This is due to the pressure staying above the lowest delivery pressure of the fuel cell for a longer period of time, in this case 1 atm. Of course, eventually the metal hydride bed will begin to run out of hydrogen and the pressure will decrease below this minimum operating pressure no matter how high the temperature.

It is interesting that the temperatures of the metal hydride bed for the coupled and uncoupled cases both exhibit sawtooth patterns but oscillate 180° out of phase with each other, i.e., when the temperature is increasing in one case it is decreasing in the other case and vice versa. Not surprisingly, the thermal energy imparted to these beds also shows these opposite behavior, but with drastically different patterns. For the uncoupled case, the temperature of the metal hydride bed initially decreases from 296 K to 291 K during the first high power cycle; thereafter, it exhibits 2 K swings in temperature between 293 K and 291 K, always being below the ambient temperature of 296 K. Hence, energy is always being transferred to the bed, a favorable effect as explained below. The periodic decreases in temperature occur when the pulsed power source draws 200 W from the fuel cell; in contrast, when only 100 W of power are drawn, the temperature increases. The opposite behavior is exhibited by the thermal power transferred to the metal hydride bed from the ambient environment. Initially, about 2.7 W are transferred at most to the metal hydride bed and then the thermal power oscillates between 2.7 W and 1.5 W when the temperature of the metal hydride bed is lowest and highest, respectively. This coupled

and 180° out of phase behavior between the temperature of and the thermal energy transferred to the bed is explained by the metal hydride bed cooling when it releases hydrogen [12]. The greater this decrease in temperature, the greater the driving force for heat transfer between the bed and the ambient environment, the greater the power input to the bed. So when the bed periodically heats back up to 293 K, the driving force for heat transfer decreases, which causes the power input to decrease. Nevertheless, the energy transferred to the bed when only 100 W are being drawn from the fuel cell is apparently enough to overcome the endothermic process associated with the release of hydrogen at the lower flow rate demand and cause it to heat back up to 293 K. However, when the power source draws 200 W and the hydrogen flow rate demand correspondingly increases to the higher value, although the energy transferred to the bed increases, it is not enough to overcome the endothermic process associated with the release of this increased amount of hydrogen. Hence, the bed cools during this period to about 291 K. This periodic behavior continues over the 4 h of operation of the fuel cell.

Similar temperature change and corresponding driving force arguments are made to describe the behavior of the coupled system. However, in this case, the 3.7–2.7 W of power imparted to the bed during high power operation is apparently enough to offset the endothermic cooling effect mentioned above because the temperature of the bed actually increases during this part of the cycle. This necessarily causes the thermal power transferred to the bed to decrease during the same period, because although the fuel cell temperature is at its high value, it essentially remains constant during this period. At the onset of low power operation, the temperature of the fuel cell decreases instantaneously to its low value (Fig. 7), which lowers the thermal power input to the metal hydride bed to about 0.5 W due to the small driving force for heat transfer. This allows the endothermic effect to begin to dominate even though the hydrogen demand is low and the temperature of the metal hydride bed begins to decrease. Nevertheless, the thermal power input to the bed increases during this period to about 1.5 W because the driving force for heat transfer now increases due to the decrease in the metal hydride bed temperature with the fuel cell temperature essentially remaining constant. This periodic behavior continues over the 4 h of operation of the fuel cell; however, the periodic behavior is clearly and subtly different when compared to the uncoupled case.

5. Conclusions

The overall objective of this paper was to study the behavior of a thermally coupled hydrogen storage and fuel cell system. An underlying and more specific objective was to determine the effect of transferring waste (thermal) energy from the fuel cell to the metal hydride bed in a truly dynamic and coupled fashion. These objectives were met by formulating dynamic models of a metal-hydride hydrogen storage system and a PEM fuel cell stack for easy implementation in the virtual test bed (VTB) environment, a simulation platform designed for carrying out systems level modeling like the integrated fuel cell system.

An inherently nonlinear model that realistically accounts for heat and mass transfer resistances associated with the discharge of hydrogen from a metal hydride bed was reformulated in a resistive companion (RC) form and successfully validated against experimental discharge data. The RC form of the metal hydride bed model was then coupled with a relatively simple, experimentally validated, PEM fuel cell model. These coupled models were used to carry out dynamic simulations of the integrated fuel cell system in the VTB environment. Two specific situations were studied: in the first scenario, the fuel cell and metal hydride bed were thermally coupled; in the second scenario, they were thermally uncoupled.

The results from these simulations clearly revealed unique and subtle behavior associated with thermally coupled systems that could not be easily gleaned from simulating each device alone as revealed from studying the uncoupled case. For example, the results exemplified the importance of providing energy to the metal hydride bed to facilitate the removal of hydrogen during a discharge process. Although a substantial amount of energy in the form of waste heat tends to be available from a PEM fuel cell to increase the temperature of the metal hydride bed during discharge, this work showed that in some cases, very little energy may be needed to make a substantial difference in the performance of the metal hydride bed. A relatively small increase in the operating temperature of the metal hydride bed, which occurred for the thermally coupled scenario, had a significant and positive effect on increasing the pressure in the metal hydride bed. This sustained higher pressure necessarily improves the utilization of stored hydrogen because the pressure of the bed is able to stay above the lowest operating pressure of the fuel cell for a longer period of time. This, in turn, translates into a longer operating time for the fuel cell. A detailed parametric study is forthcoming.

Acknowledgments

This work was supported in part by the US Army CECOM under contract NRO-00-C-0134, and by US ONR under contract N00014-00-1-0368 and under contract N00014-99-1-0560.

References

[1] Y. Baghzouz, J. Fiene, J.V. Dam, L. Shi, E. Wilkinson, R. Boehm, Progress on improvements to a hydrogen/electric hybrid bus, in: Proceedings of the 2000 Hydrogen Program Review.
[2] K.S. Jeong, B.S. Oh, J. Power Sources 105 (2002) 58–65.
[3] J.A. Ritter, A.D. Ebner, J. Wang, R. Zidan, Mater. Today 9 (2003) 18–23.

[4] V. Guther, A. Otto, J. Alloys Compd. 293/295 (1999) 889–892.
[5] S. Lévesque, M. Ciureanu, R. Roberge, T. Motyka, Int. J. Hydrogen Energy 25 (2000) 1095–1105.
[6] L.K. Heung, On-board hydrogen storage system using metal hydride, hydrogen power: theoretical and engineering solutions., in: Proceedings of the HYPOTHESIS Symposium, vol. 2, Grimstad, Norway, August 18–22, 1997, pp. 251–256.
[7] A. Jemni, S.B. Nasrallah, J. Lamloumi, Int. J. Hydrogen Energy 24 (1999) 631–644.
[8] B. Wu, R.E. White, J. Electrochem. Soc. 148 (2001) 595–609.
[9] H.B. Kang, W.C. Park, S.C. Lee, Int. J. Hydrogen Energy 21 (1996) 769–774.
[10] S.A. Gadre, A.D. Ebner, S.A. Al-Muhtaseb, J.A. Ritter, Ind. Eng. Chem. Res. 42 (2003) 1713–1722.
[11] M.L. Blackweider, PEM Fuel Cell VTB Model Help File, available on-line at: http://vtb.engr.sc.edu/models/index.asp.
[12] R.A. Dougal, T. Lovett, A. Monti, E. Santi, A multi-language environment for interactive simulation and development of controls for power electronics, in: IEEE Power Electronics Specialists Conference, Vancouver, Canada, June 17–22, 2001.
[13] G. Cokkinides, B. Beker, VTB Model Developer's Guide, available on-line at: http://vtb.engr.sc.edu/modellibrary/modeldev.asp.
[14] G. Cokkinides, B. Beker, RC and AC Models in the VTB Time Domain Solver, The VTB Documentation, December 04, 1998.
[15] M.R. Gopal, S.S. Murthy, Int. J. Hydrogen Energy 20 (1995) 911–917.
[16] S. Lee, H. Lee, K. Lee, J. Lee, J. Alloy Compd. 234 (1996) 84–92.
[17] Z. Guo, H.J. Sung, Int. J. Heat Mass Transfer 42 (1999) 379–382.
[18] J. Kim, S.M. Lee, S. Srinivasan, J. Electrochem. Soc. 142 (1995) 1670–2674.
[19] Y. Zhang, M. Ouyang, W. Lu, J. Luo, X. Li, Appl. Therm. Eng. 24 (2004) 501–513.
[20] J.C. Amphlett, R.F. Mann, B.A. Peppley, P.R. Roberge, A. Rodrigues, J. Power Sources 61 (1996) 183–188.